CRYSTAL GROWTH & DESIGN

Article

pubs.acs.org/crystal

Influential Role of Geometrical Disparity of Linker and Metal Ionic Radii in Elucidating the Structural Diversity of Coordination Polymers Based on Angular Dicarboxylate and Bis-pyridyl Ligands

Paulami Manna, Bharat Kumar Tripuramallu, and Samar K. Das*

School of Chemistry, University of Hyderabad, P.O. Central University, Hyderabad, 500046, India

Supporting Information

ABSTRACT: As a continuation of our recent investigations on coordination polymer/metal−organic framework containing compounds, herein, four new coordination polymers, namely, $\{Co_2(ADA)_2(px2ampy)\}_n$ (**1**), $\{Cd(ADA)(px2ampy)_{0.5}\}_n$ (**2**), $\{Co_2(IPTA)_2(px2ampy)\}_n$ (**3**), $\{Mn(IPTA)(px3ampy)\}_n$ (**4**) have been synthesized, based on the flexible dicarboxylate ligand H_2ADA and rigid dicarboxylate ligand H_2IPTA along with long flexible bis-pyridyl linkers as coligand (where H_2ADA = 1,3-adamantanediacetic acid; H_2IPTA = isopthalic acid; px2ampy = 1,4-bis(2-pyridylaminomethyl)benzene; px3ampy = 1,4-bis(3-pyridylaminomethyl)benzene). Compounds **1**−**4** have been characterized by routine elemental analysis, IR spectroscopy, and thermogravimetric (TG) analysis and unambiguously by single crystal X-ray diffraction analysis. The solid-state luminescent property of compound **2** has been additionally characterized. Compound **1** is a two-dimensional (2D) framework, constructed by the connectivity of Co_2 paddle-wheels as secondary building units (SBUs) and the organic linkers. The 2D sheet of compound **2** consists of Cd-dimers as SBUs and extends to a supramolecular three-dimensional (3D) framework through H-bonding interactions among the sheets. Compound **3** is a 3D coordination polymer, in which an unusual SBU is formed by two Co^{II} centers: one in tetrahedral and the other one in octahedral coordination geometries. In the crystal structure of compound **4**, the connectivity of the Mn_2-dimers with the macrocyclic rings, formed from px3ampy coligands, results in the formation of 2D layer structures. The title compounds **1**−**4** illustrate an important structural relationship, which can be rationalized by the geometrical diversity of two different dicarboxylate ligands and the nature of different metal ions, employed in this study. The role of the metal ionic radii in assessing the formation of final architectures, thereby, influencing the dimensionality of the compounds has been discussed. The long flexible pyridyl spacers, present in all these compounds as an integral part, modulate themselves in different conformations depending on the requirement of the coordination environment.

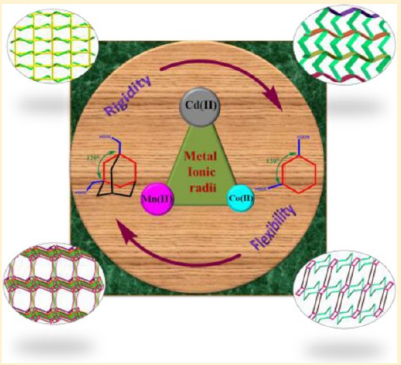

INTRODUCTION

Coordination polymers, especially the metal organic framework (MOF) containing compounds, rapidly came into focus in modern inorganic chemistry with immense interest because of their potential applications as storage medium for gases and promising applications for separation and purification.[1] Moreover, having the combining power of both the inorganic and organic components, MOFs are blessed with some unique properties and uses in the areas of magnetism,[2] luminescence,[3] catalysis,[4] etc. In general, there is a correlation between the complexity of the structure and functionality of the material.[5] The constant evolution of complexity of coordination polymers in terms of functionality requires more knowledge of synthetic strategies to understand the structures. In order to model the functional crystalline solids with desired properties, considerable efforts have been devoted to understand the self-assembly process of the coordination networks.[6] In this context, numerous coordination polymers have been reported by utilizing the multitopic building blocks, such as carboxylates,[7] phosphonates,[8] sulfonates,[9] organonitrogen bridging ligands, terminal aromatic chelating ligands,[10] etc.

The rigidity and flexibility of the organic linkers, involved in the construction of coordination networks, have a great impact in modulating the functional properties of the networks in the concerned compounds.[11] In recent times, the flexible linkers are often used to build fascinating structures owing to impacting their functionalities to the coordination networks. The flexibility can be introduced either in the skeleton of the linker or as a substituent to the linker; both methods offer a promising approach in achieving flexible coordination networks. Fischer et al. recently reported the breathing behavior of pillared-layered MOFs through functionalized linkers bearing flexible substituents.[12] Molecular recognition and solid state breathing are the major attributes of the coordination polymers that are build by flexible linkers. On the other hand, rigid linkers can predict coordination patterns, in contrast to the flexible ligands. In dual ligand systems, metal-carboxylate architectures can be finely tuned by incorporating the different secondary N-donor linkers.

Received: October 10, 2013
Revised: November 4, 2013
Published: November 12, 2013

dx.doi.org/10.1021/cg401502f | *Cryst. Growth Des.* 2014, 14, 278−289

Scheme 1. Diagram of the Synthetic Strategy for the Compounds Presented in This Article

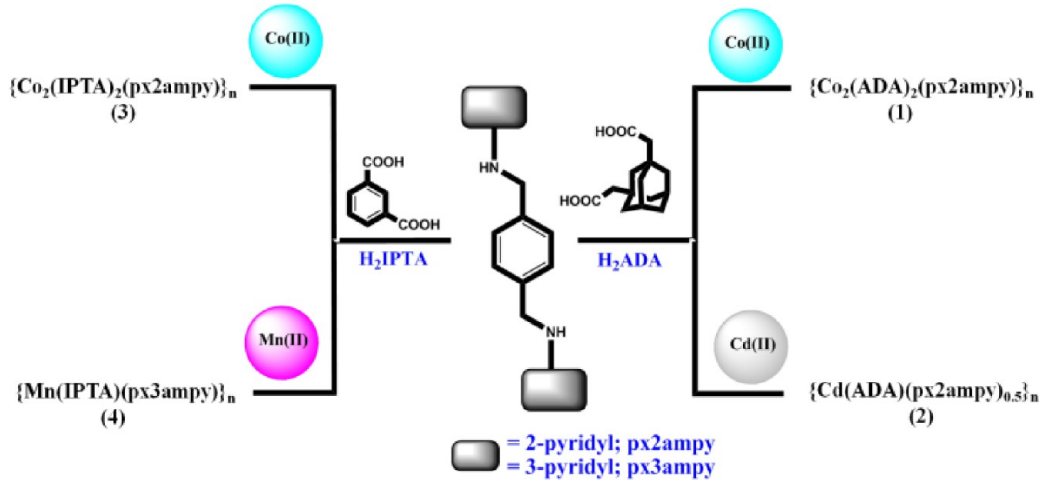

The geometry of the secondary N donor linker mediated conformational modulation of the flexible carboxylates is reported with several examples in the literature.[13] When these linkers are used to build coordination networks, several factors have to be addressed, such as noncovalent interactions (which are responsible for breathing behavior of the concerned material), metal ion coordination sphere (for tuning dimensionality), geometry of the secondary linker (for mediating conformational modulation), etc. A comprehensive study encompassing all these primary factors would be necessary in analyzing the versatile networks in the concerned materials. In this regard, our motto is to reduce the complexity in designing the system and utilize the system toward functional applications. We have been working on such studies recently and proposed some noteworthy features in the exploration of flexible ligands.[14]

Among the various ditopic polycarboxylate systems, angular carboxylate linkers have intriguing characteristics compared to other systems to build coordinating networks.[15] A wide variety of angular carboxylate linkers are well explored in the literature, where the linker coordination angle of 120° has been kept constant and the peripherals of the skeleton have been changed. These angular linkers tend to facilitate the formation of helical structures or interpenetrated double layers due to their folded conformations.[16] The attachment of flexibility, provided by the $-CH_2-$ group in the skeleton to the angular linkers, would be more appropriate for the formation of helical coordination polymers.[17] The knowledge of the coordination domain (around the metal ion) of these angular ligands, that may be of flexible, rigid, planar, bent, and/or twisted geometries, is still remains in the infancy stage with a very few reports in the literature. This offers a lot of scope to increase the potentiality of such system (flexibility of angular linkers, coordinated to the metal) by exploring the versatility of these linkers to build interesting helical, meso-helical, and zigzag coordination networks. On the other hand, the transitional metal ionic radii have a synergetic effect on the subtle conformation of the linker in assembling the coordination frameworks.

In this article, we have chosen H_2ADA,[18] a flexible nonplanar angular ligand, and H_2IPTA,[19] a rigid planar angular linker, as main organic building units to extend our ongoing studies. It is important to note that the adoptability of different torsion angles by acetate groups, nonplanar twisted conformation of H_2ADA linker and the rigidity, planarity of H_2IPTA linker for forming determined orientation of coordination geometries contrast these linkers from other customary dicarboxylate linkers. The structural similarity of these two angular linkers (H_2ADA and H_2IPTA) has been considered as a token of advantage to explore their comparative coordination patterns in connection with secondary linkers. The longer flexible pyridyl linkers[20] of higher degree (in terms of flexibility) are employed in combination with H_2ADA or H_2IPTA linker, and we have studied their coordination consequences in forming diverse architectures. We have chosen rationally based on metal ionic radii, Co(II), Cd(II) metals to synthesize compounds $\{Co_2(ADA)_2(px2ampy)\}_n$ (**1**), $\{Cd(ADA)(px2ampy)_{0.5}\}_n$ (**2**) and Co(II), Mn(II) for compounds $\{Co_2(IPTA)_2(px2ampy)\}_n$ (**3**), $\{Mn(IPTA)(px3ampy)\}_n$ (**4**) respectively (see also Scheme 1). All these compounds are synthesized under hydrothermal conditions and structurally characterized by single crystal X-ray diffraction. The phase purity has been determined by powder X-ray diffraction studies.

EXPERIMENTAL SECTION

Materials and Methods. All the chemicals were received as reagent grade and used without any further purification. The ligand px2ampy was prepared according to the literature procedures.[21] Elemental analyses were determined by FLASH EA series 1112 CHNS analyzer. Infrared spectra of solid samples obtained as KBr pellets on a JASCO 5300 FT-IR spectrophotometer. Thermogravimetric analyses were carried out on a STA 409 PC analyzer, and corresponding masses were analyzed by QMS 403 C mass analyzer, under flow of N_2 gas with a heating rate of 5 °C min^{-1}, in the temperature range of 30−1000 °C. Powder X-ray diffraction patterns were recorded on a Bruker D8-Advance diffractometer using graphite monochromated Cu $K_{\alpha 1}$ (1.5406 Å) and $K_{\alpha 2}$ (1.54439 Å) radiations. The emission spectrum of compound **2** in the solid state was recorded at room temperature on a Horiba Jobin Yvon Fluoromax-4 spectrofluorometer. All the compounds were synthesized in 23 mL Teflon-lined stainless vessels (Thermocon, India) under hydrothermal conditions.

Synthesis of $\{Co_2(ADA)_2(px2ampy)\}_n$ (1). A mixture of $CoCl_2 \cdot 6H_2O$ (0.25 mmol, 59.5 mg), H_2ADA (0.25 mmol, 63.3 mg), and px2ampy (0.25 mmol, 72.5 mg) in H_2O/MeOH (10:2) was stirred for 30 min and sealed in a 25 mL Teflon-lined stainless steel autoclave (pH = 7.20). The reaction mixture was heated at 130 °C for 4 days and then slowly cooled to room temperature. Deep red block crystals were obtained. Yield: 47.6% (based on Co). Anal. Calcd for $C_{46}H_{30}Co_2N_4O_8$ (M_r = 904.76): C, 61.06%; H, 5.57%; N, 6.19%. Found: C, 62.25%; H, 5.73%; N, 6.73%. IR (KBr pellet, cm^{-1}): 3391,

dx.doi.org/10.1021/cg401502f | Cryst. Growth Des. 2014, 14, 278−289

Table 1. Crystal Data and Structural Refinement Parameters for Compounds 1−4

	1	2	3	4
empirical formula	$C_{46}H_{50}Co_2N_4O_8$	$C_{23}H_{27}CdN_2O_4$	$C_{34}H_{26}Co_2N_4O_8$	$C_{26}H_{19}MnN_4O_4$
formula weight	904.76	507.88	736.45	506.39
T (K) /λ (Å)	298(2)/0.71073	298(2)/0.71073	298(2)/0.71073	298(2)/0.71073
crystal system	monoclinic	triclinic	orthorhombic	triclinic
space group	$P2_1/c$	$P\bar{1}$	$Pca2(1)$	$P\bar{1}$
a (Å)	12.7076(11)	10.031(2)	21.298(4)	10.062(6)
b (Å)	20.6676(19)	10.219(2)	9.884(2)	10.289(6)
c (Å)	16.6371(15)	10.793(2)	14.823(3)	12.659(7)
α (°)	90.00	85.53(3)	90	88.328(9)
β (°)	106.908(2)	82.09(3)	90	73.347(8)
γ (°)	90.00	75.37(3)	90	64.570(8)
volume (Å^3)	4180.6(6)	1059.2(4)	3120.3(11)	1127.2(11)
Z, ρ_{calcd} (g cm^{-3})	4, 1.437	2, 1.592	4, 1.568	2, 1.492
μ (mm^{-1}), F(000)	0.566/566	0.688/1188	1.124/1504	0.628/520
goodness-of-fit on F^2	1.082	1.092	1.080	1.090
R_1/wR_2 [$I > 2\sigma(I)$]	0.0582/0.1239	0.0233/0.0593	0.0333/0.0649	0.0371/0.1060
R_1/wR_2 (all data)	0.0798/0.1339	0.0255/0.0607	0.0391/0.0680	0.0429/0.1242
largest diff peak/hole (e Å^{-3})	0.650/−0.332	0.314/−0.360	0.522/−0.287	0.643/−0.605

3369, 2915, 2895, 1616, 1578, 1539, 1441, 1402, 1331, 1145, 1013, 767, 684, 438.

Synthesis of {Cd(ADA)(px2ampy)$_{0.5}$}$_n$ (2). The same synthetic method as that for compound **1** was used to obtain the compound **2**, except that $CoCl_2{\cdot}6H_2O$ was replaced by $CdCl_2{\cdot}H_2O$ (0.25 mmol, 59.5 mg) and methanol was not added in the reaction mixture. Block-shaped colorless crystals of **2** were collected in 59% yield (based on Cd). Anal. Calcd for $C_{23}H_{27}CdN_2O_4$ (M_r = 507.88): C, 54.39%; H, 5.35%; N, 5.51%. Found: C, 55.02%; H, 5.74%; N, 5.12%. IR (KBr pellet, cm^{-1}): 3408, 3237, 2899, 1665, 1614, 1588, 1535, 1440, 1385, 1327, 1164, 967, 792, 712.

Synthesis of {Co$_2$(IPTA)$_2$(px2ampy)}$_n$ (3). The same synthetic procedure, as that of compound **1**, was followed to obtain the compound **3** except ligand H_2IPTA (0.25 mmol, 41.5 mg) was used in place of H_2ADA, and pH of the solution was maintained at 8.00. Blue block crystals of **3** were obtained in 45% yield (based on Co). $C_{34}H_{26}Co_2N_4O_8$ (M_r = 736.45): C, 55.45%; H, 3.558%; N, 7.607%. Found: C, 55.71%; H, 3.83%; N, 7.36%. IR (KBr pellet, cm^{-1}): 3352, 3193, 2850, 1684, 1450, 1340, 1234, 1102, 825, 752, 692, 654.

Synthesis of {Mn(IPTA)(px3ampy)}$_n$ (4). We synthesized the compound **4** following the similar synthetic pathway as above using the $Mn(OAc)_2{\cdot}4H_2O$ (0.25 mmol, 61.25 mg), H_2IPTA (0.25 mmol, 41.5 mg), and px3ampy (0.25 mmol, 72.5 mg). Light pink color crystals were filtered off with 60% yield (based on Mn). $C_{26}H_{19}MnN_4O_4$ (M_r = 506.39): C, 61.67%; H, 3.781%; N, 11.063%. Found: C, 61.21%; H, 3.56%; N, 10.87%. IR (KBr pellet, cm^{-1}): 3340, 2967, 2863, 1710, 1475, 1354, 1210, 1150, 995, 845, 754, 698, 649.

Single Crystal X-ray Structure Determination of the Compounds 1−4. Single-crystals, suitable for structural determination of compounds **1**−**4**, were mounted on a three circle Bruker SMARTAPEX CCD area detector system under Mo Kα (λ = 0.71073A) graphite monochromated X-ray beam with crystal to detector distance 60 mm, and a collimator of 0.5 mm. The scans were recorded with an ω scan width of 0.3°. Data reduction was performed by SAINTPLUS,[22a] empirical absorption corrections were done using equivalent reflections performed by program SADABS;[22b] structure solution performed using SHELXS-97[22c] and full-matrix least-squares refinement using SHELXL-97[22d] for above compounds. All the non-hydrogen atoms were refined anisotropically. Hydrogen atoms on the C atoms were introduced on calculated positions and were included in the refinement riding on their respective parent atoms. Crystal data, structure refinement parameters for all the compounds (**1**−**4**) are summarized in Table 1, and complete bond lengths, bond angles are presented in the Section-3 of Supporting Information. Topological analysis of the compounds are performed by using the TOPOS software.[22e]

RESULTS AND DISCUSSION

Synthesis. The hydrothermal techniques have been employed extensively in the synthesis of coordination polymers (or metal−organic frameworks) because heating a reaction mixture in a sealed vessel/container offers reaction temperatures greater than the boiling point of the pertinent solvent under autogenous pressure. The superheated solvents exhibit reduced viscosity which enhances the diffusion of concerned chemical species and show very different solubilizing properties compared to ambient conditions. Hence, in this work we are motivated to adopt the solvothermal technique for synthesizing the coordination polymer-/MOF-type compounds in the form of single crystals for their unambiguous characterization. In order to obtain single crystals with good yield, we carried out a series of experiments to choose the suitable reaction temperature, reaction time, type of solvent, pH, and compositional metal to ligand ratio. An optimized condition of heating the composition metal/acid/N-donor linker with a 1:1:1 ratio at 130 °C for 4 days was established to produce the good quality and good amount of crystals in the present study, where, we adjusted the pH of the reaction mixture in the range 7.00−8.00 to deprotonate the H_2ADA ligand. In this pH range, both the acid ligands H_2ADA and H_2IPTA lose their both protons and present as completely deprotonated forms ADA^{2-} and $IPTA^{2-}$ in the crystal structures of compounds **1**, **2** and **3**, **4** respectively. We intended to make their singly deprotonated forms $HADA^{1-}$ and $HIPTA^{1-}$ by maintaining relatively lower pH of the reaction mixture, but we ended up with microcrystalline precipitate, which could not be characterized unambiguously. Although we have synthesized compounds **1**−**4** in an aqueous medium, but in case of compound **1** better yield was obtained by adding 2.0 mL methanol in the reaction system. All these compounds show air stability and water insolubility.

Description of Crystal Structures. *{Co$_2$(ADA)$_2$(px2ampy)}$_n$ (1).* The result of the crystallographic analysis reveals that compound **1** crystallizes in monoclinic space group $P2_1/c$. In the relevant crystal structure, there is a two-dimensional (2D) Co-ADA grid-like structure interwoven with N-donor ligand px2ampy. The molecular structure consists of a very well-known cobalt paddle-wheel (Figure

dx.doi.org/10.1021/cg401502f | Cryst. Growth Des. 2014, 14, 278−289

1a) as a secondary building unit (SBU). Both the Co(II) atoms, in the paddle-wheel, are in a distorted octahedral geometry

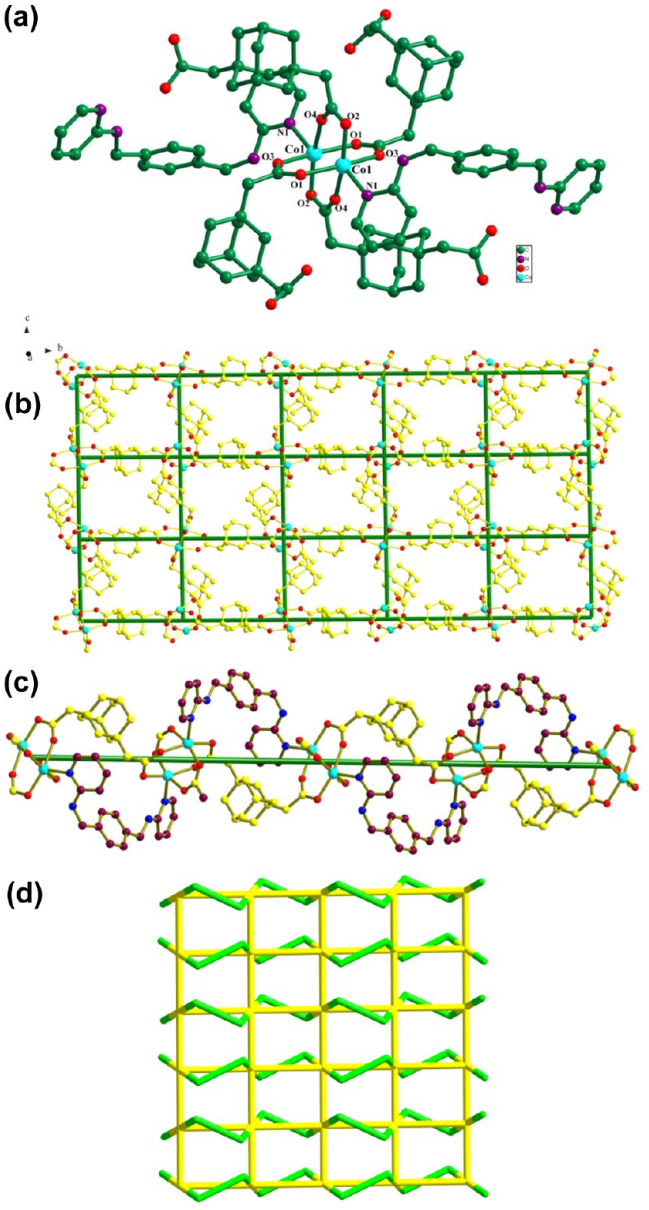

Figure 1. (a) Coordination environment around the Co(II) in compound **1**; hydrogen atoms are omitted for clarity. (b) 2D (4,4) connected network formed due to connectivity of Co(II) with ADA^{2-} ligands. (c) The connectivity of L1 with Co-ADA along the *b* axis. (d) Topological representation of 2D metal-acid layers interwoven by the L1 ligand.

(considering a metal−metal bond), in which four carboxylate oxygen atoms are connected to a Co(II) ion along the equatorial plane with average Co−O distances of 2.055 Å and a pyridyl nitrogen atom at one of the apical positions with a Co−N distance of 2.087 Å. A pair of Co(II) ions are bridged by four carboxylate groups from four different ADA^{2-} anions to form $\{Co_2(COO)_4\}$ paddle-wheel with Co···Co separation of 2.875 Å. The metal atoms, in the paddle-wheel, are bridged by the ADA^{2-} anion in a tetradentate coordination mode (both carboxylate groups on either sides of the linker adopt a bidentate μ_2-η^1:η^1 mode) as shown in Figure 1a. In the relevant crystal structure, each $\{Co_2(COO)_4\}$ dimer acts as a four-connector node and connects to the other four surrounding paddle-wheels using four ADA^{2-} linkers and two px2ampy linkers to form a 2D grid-like layer along the crystallographic *bc* plane (Figure 1b). The connectivity of the paddle-wheels with ADA^{2-} leads to the formation of single-strand mesohelical chains with alternating left and right turns of the strand along the crystallographic *b* and *c* axes, which results in the formation of a 2D metal acid layer. The resulting metal acid layer consists of two different pairs of ADA^{2-} linkers which differ mainly in terms of their torsion angles between the acetate groups. A pair of ADA^{2-} ligands having the torsion angle of 100.17° (viewed through C1−C2−C13−C14) between two acetate groups creates a separation of 8.319 Å between two paddle-wheels along the crystallographic *c* axis and the other set with a torsion angle of 118.86° (viewed through C15−C16−C27−C46) connects through crystallographic *b* axis resulting in a separation 10.334 Å between the two paddle wheels. The dimension of the resulting grid motif is 13.266 × 13.266 Å (considering the diagonal distance). Additionally, the ligand px2ampy implements the *cis*−*trans*−*trans* conformation[14b] forming a one-dimensional (1D) zigzag chain by connecting the paddle-wheel units along the *b* axis (Figure 1c), where ADA^{2-} creates a separation of 10.334 Å between the two paddle-wheels; along the other axis (i.e., along the *c* axis), the coordination of px2ampy ligiand is absent. The connectivity of the Co−px2ampy chains can be viewed as the "sewing" the metal-acid layers with the thread of px2ampy (Figure 1d). Generally the metal acid layers, with the involvement of a long linker, can be pillared, but in the present study (compound **1**), the linker px2ampy, instead of pillaring the layers, adopts a planar coordination. This unusual coordination mode of px2ampy does not favor the formation of a three-dimensional (3D) structure. The topology of the 2D sheets can be described, in brief, by considering the $\{Co_2(COO)_4\}$ paddle-wheel units as nodes and ADA^{2-} as linkers forming a (4,4) connectivity.

$\{Cd(ADA)(px2ampy)_{0.5}\}_n$ (***2***). Structural analysis indicates that compound **2** is a 2D ladder structure and crystallizes in the triclinic $P\bar{1}$ space group. The relevant asymmetric unit consists of one crystallographically independent Cd(II), one completely deprotonated ADA^{2-}, and half of the px2ampy ligand. As shown in Figure 2a, the Cd(II) center is located in a severely distorted$\{CdNO_5\}$ octahedral geometry, completed by the five carboxylate oxygen atoms from three different ADA^{2-} ligands and one pyridyl nitrogen atom from the px2ampy ligand. The Cd−O bond lengths are in the range of 2.242−2.394 Å, the Cd−N bond length is 2.265 Å, and the bond angles around the Cd(II) center are in range of 54.66−123.1°. Two carboxylate groups of the ADA^{2-} ligand adopt two different coordination modes in this compound, resulting in the formation of different SBUs rather than regular paddle-wheel geometry. One carboxylate group of the ADA^{2-} connects in bidentate μ_1-η^1:η^1 fashion, that is, simultaneously coordinates to a single Cd(II) center through the both oxygen atoms; on the other hand, the other carboxylate group connects in a bridging tridentate coordination mode μ_2-η^2:η^1, whereby both the oxygen atoms coordinate to one Cd(II) center in chelating mode and one of the oxygen atom of the −COO group further connected to an another Cd(II) center in bridging mode. The μ_2-η^2:η^1 coordination of carboxylate group of two different ADA^{2-} ligands results in the formation of a Cd_2O_2 dimer. These dimers are connected to each other along the length of the ADA^{2-} ligand affording double-stranded mesohelical chains of

dx.doi.org/10.1021/cg401502f | *Cryst. Growth Des.* 2014, 14, 278−289

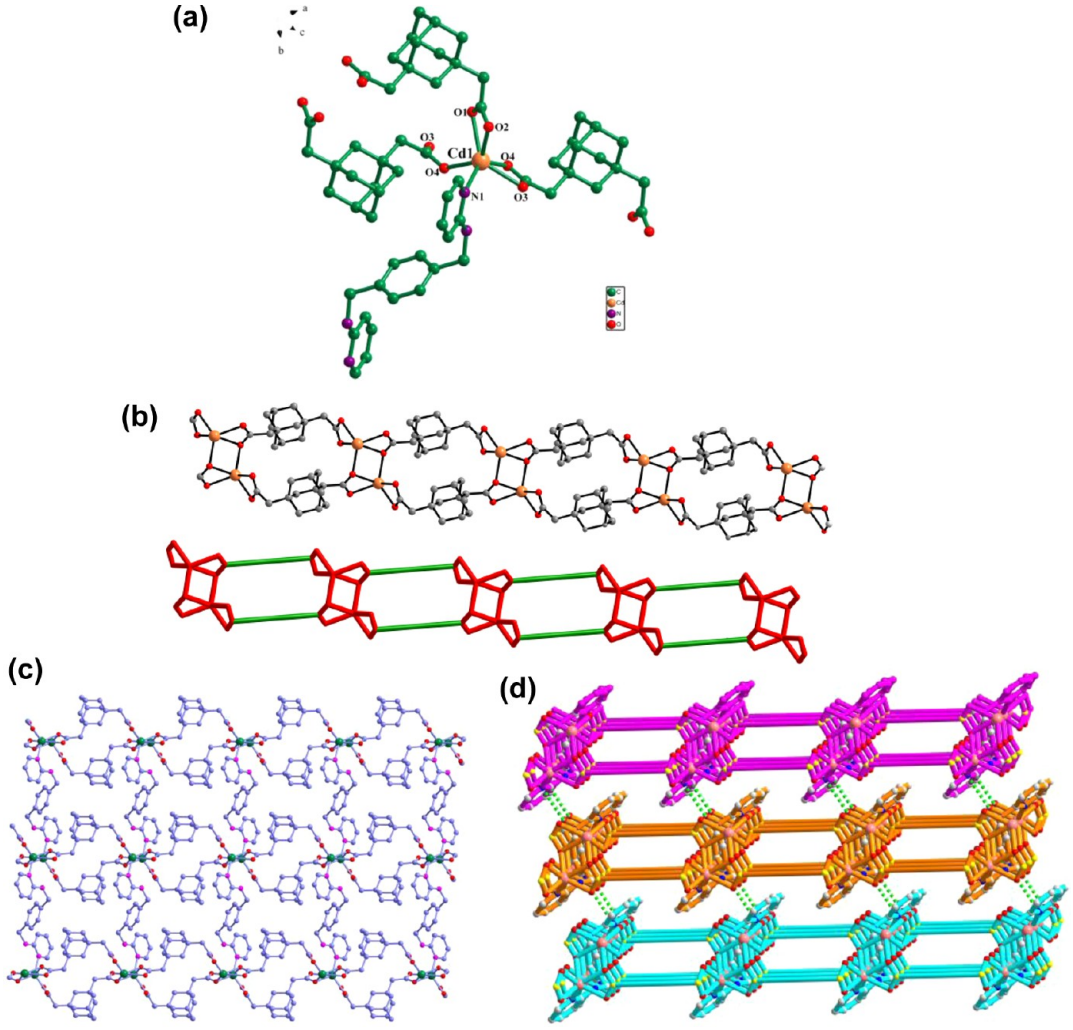

Figure 2. (a) Molecular diagram of compound **2** (b) 1D ladderlike structure formed due to connectivity of Cd(II) with ADA^{2-} linkers and its topological representation. (c) 2D layers formed due to connectivity of Cd(II)-ADA ladders with the L1 ligand. (d) Connectivity of 2D sheets through noncovalent interactions.

Cd^{II}-ADA^{2-}, which finally results in the formation of a 1D ladder-like structure along the crystallographic *c* axis (Figure 2b). In these 1D ladders, the ligand ADA^{2-} exists in *trans* configuration with a torsion angle of 166.79° (viewed through C1−C2−C13−C44) between the two acetate groups. These 1D chains are pillared by the linker px2ampy through a crystallographic *a* axis to form 2D sheets along the *bc* plane (Figure 2c). The ligand px2ampy connects the apical sites of the Cd(II) metal centers of the Cd_2O_2 dimers from two adjacent 1D ladders in a perfect *trans*−*trans*−*trans* configuration. The separation, created by the px2ampy linker, between two metal acid chains is 13.185 Å. The overall connectivity of metal-acid chains with the flexible long linker (px2ampy) results in the formation of a 2D (4,4) connected gridlike arrangement, considering Cd_2O_2 dimers as nodes and a pair of ADA^{2-} ligands as single connector and px2ampy as the other connecter. These 2D sheets are perfectly stacked one over the other in an eclipsed mode, resulting in the formation of 1D pores along the crystallographic *b* axis with a cavity size of 13.185 × 10.179 $Å^2$ (Figure 1, Sec-3 in Supporting Information). Moreover, the adjacent 2D layers interact with each other through hydrogen bonding interactions between methylene carbon hydrogen atoms of the px2ampy ligand of one layer and the N atom of the pyridine ring of the px2ampy ligand from the other layer. This C−H···N (symmetry code 1 − *x*, 1 − *y*, 2 − *z*) hydrogen bonding among the 2D layers extends the final architecture to a 3D supramolecular network (Figure 2d).

$\{Co_2(IPTA)_2(px2ampy)\}_n$ (**3**). Compound **3** crystallizes in orthorhombic space group *Pca*2(1) and the single-crystal structure analysis shows that, in the asymmetric unit (Figure 3a) of the compound **3**, two crystallographically independent Co(II) metal ions (Co1 and Co2) are presented. Co1 is characterized by a perfect octahedral geometry, coordinated with five oxygen atoms from four different $IPTA^{2-}$ ligands that occupy four equatorial positions and one of the apical positions; the rest of the apical positions is connected by the N atom from the px2ampy ligand. In $\{Co(1)O_5N\}$ octahedron, all the Co1−O bond distances are in the range of 2.054−2.184 Å, and Co1−N bond distance is 2.147 Å. The other (crystallographically independent) Co2 metal center adopts a tetrahedral geometry by accommodating three O atoms from three different $IPTA^{2-}$ ligands and one N atom from one px2ampy ligand. The bond distances around the Co2 metal center are shorter compared to those around Co1; three Co2−O bond distances (around Co2) fall in the range of 1.927−

dx.doi.org/10.1021/cg401502f | *Cryst. Growth Des.* 2014, 14, 278−289

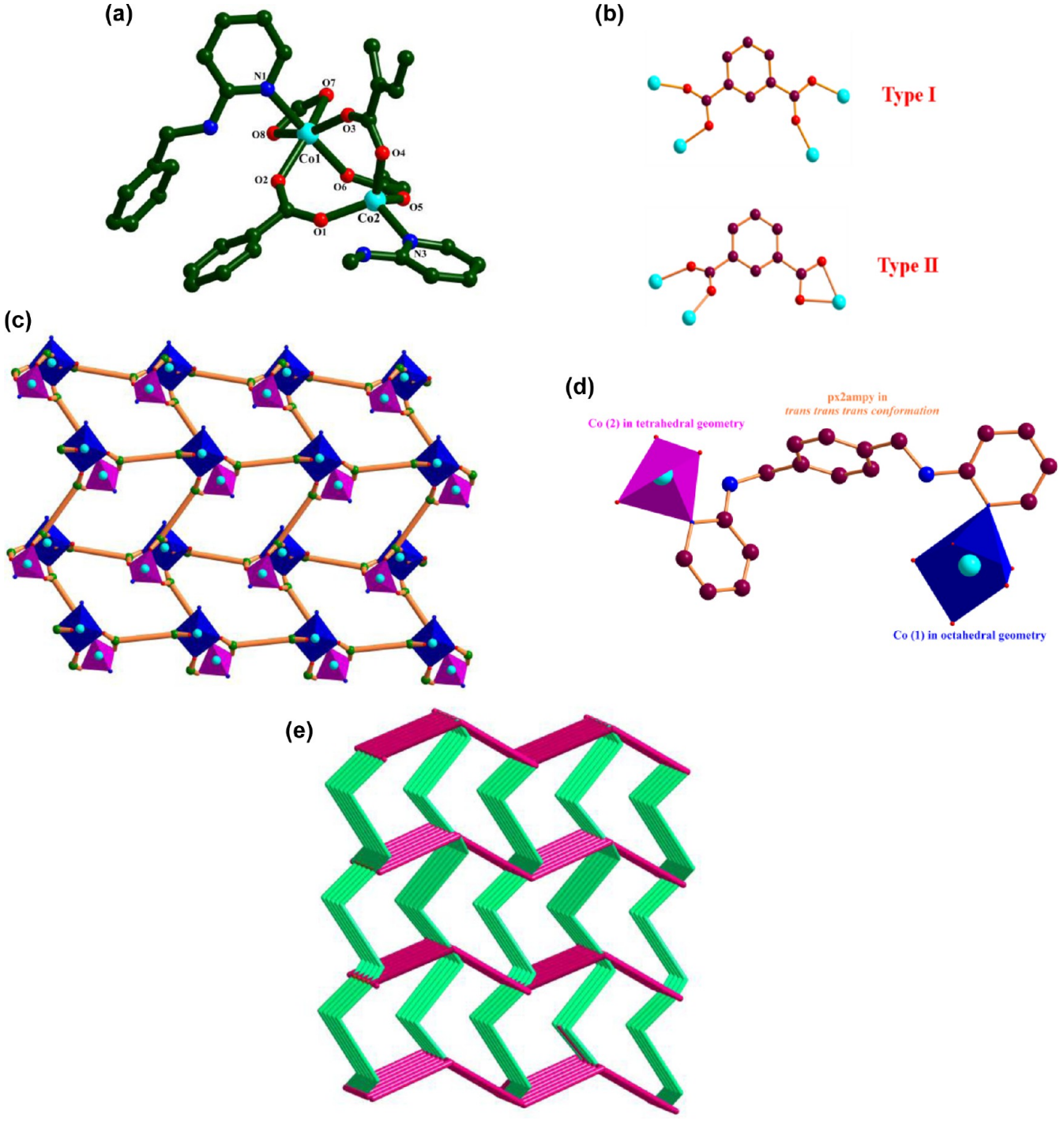

Figure 3. (a) Asymmetric unit of compound **3**, (b) connectivity of the Type I and Type acid ligand. (c) Representation of the 2D corrugated layers formed by the connectivity of the $IPTA^{2-}$ and Co-dimer. (d) Connectivity of the px2ampy linker. (e) 3D topological representation of the compound **3**.

1.937 Å, and the Co2−N bond length is 2.043 Å. These two different Co(II) metal centers are bridged by the two carboxylate groups from two different $IPTA^{2-}$ ligands in a bridging bidentate coordination mode μ_2-η^1:η^1, resulting in the formation of cobalt binuclear unit (SBU), in which the metal centers are separated from each other by a distance of 3.624 Å. These binuclear Co(II) centers (SBUs) are connected by two types of $IPTA^{2-}$ ligands (namely, Type I and Type II as shown in Figure 3b). The Type I acid ligand is present in tetradentate mode, in which both the carboxylate groups adopt the bridging bidentate μ_2-η^1:η^1 coordination mode, whereby the benzene ring and the two carboxylate groups are present in the same plane. The Type II $IPTA^{2-}$ is portrayed in another tetradentate mode, where one carboxylate group adopts the monodentate μ_1-η^1:η^1 coordination mode which is in the plane of benzene ring, but the other carboxylate group adopts the bridging bidentate μ_2-η^1:η^1 coordination mode which is twisted from the plane of the benzene ring by a angle of 40.26° (Figure 3b). The binuclear Co(II)-SBUs are connected by Type II acid ligand (Figure 3b) along the crystallographic *b* axis to form a 1D chain

dx.doi.org/10.1021/cg401502f | *Cryst. Growth Des.* 2014, 14, 278−289

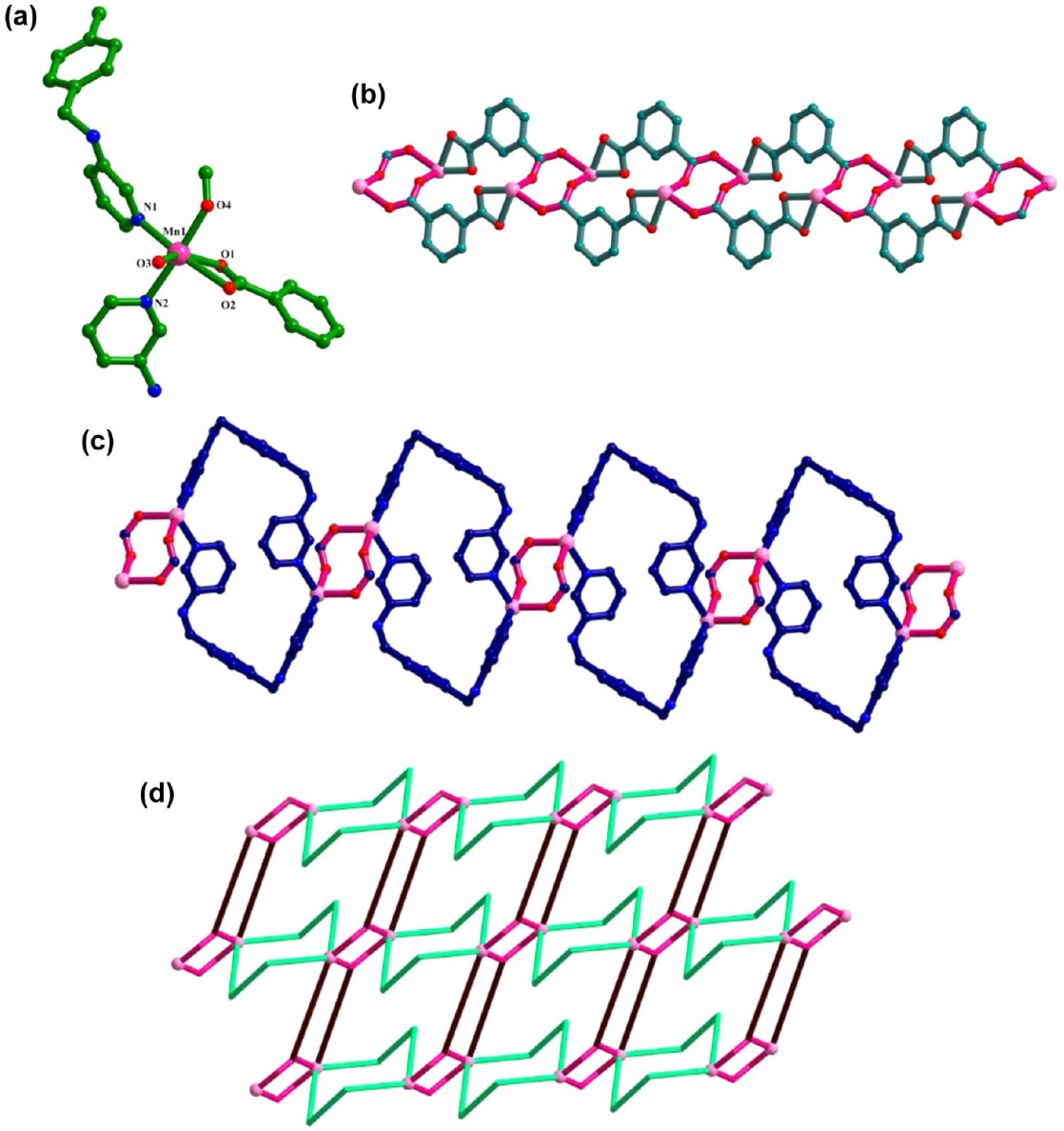

Figure 4. (a) Asymmetric unit of compound **4** with coordination sphere labeling. (b) 1D chain constructed by the connectivity of Mn_2 dimer and $IPTA^{2-}$. (c) Arrangement of the macrocycles ring formed by the px3ampy. (d) 2D topological representation of the compound **4**.

in which all the metal atoms are coplanar, and the benzene rings of the acid are present in a different plane deviated from the plane containing metal atoms. On the other hand, the Type I acid ligand (Figure 3b) connects the SBUs to form Co−Type II acid chains along the crystallographic *c* axis in a zigzag fashion with dihedral angle of 73.04° (between the two type of acid planes), and also the SBUs are aligned alternatively in opposite direction. These features do not allow the dwelling of all the Co_2 dimers (SBUs) in the same plane, rather in two different planes, where the Co_2 units are distributed/arranged alternatively. The associate connectivity of binuclear Co(II) units with these two types of $IPTA^{2-}$ ligands generate a 2D (4,4) connected grid-like metal-acid corrugated sheets (Figure 3c). The adjacent 2D sheets are further connected by secondary linker px2ampy in a *trans*−*trans*−*trans* conformation by creating a separation of 10.66 Å to form a layered pillared 3D framework. The px2ampy linker connects the Co(II) atoms, belonging to the Co_2 dimers, between the adjacent layers in a weird fashion, in which the pyridyl nitrogen atom of one end of the linker coordinates to the Co(II) center, which has octahedral geometry, and the other end of the linker is attached to the Co(II) center, which has ta etrahedral coordination sphere as shown in the Figure 3d. The overall connectivity of the 2D metal acid sheets with the px2ampy linkers results in the formation of a 3D framework. The topology of 3D framework can be defined as a (7,9)-connected with $(3^7 \cdot 4^8 \cdot 5^2 \cdot 6^4)(3^8 \cdot 4^{16} \cdot 5^4 \cdot 6^8)$ topology (Figure 3e).

*{Mn(IPTA)(px3ampy)}$_n$ (**4**).* Single crystal determination of compound **4** reveals a 2D framework, constituted by the $IPTA^{2-}$ ligand and the flexible px2ampy linker. Compound **4** crystallizes in triclinic space group $P\bar{1}$. The relevant asymmetric unit consists of one Mn(II) ion, one $IPTA^{2-}$ ligand, and one px3ampy ligand as shown in the Figure 4a. Each Mn(II) metal center is surrounded by four O atoms from three $IPTA^{2-}$ anions and two N atoms of pyridine ring from two different px3ampy linkers affording a distorted octahedral coordination sphere around the metal ion. All the Mn−O/Mn−N bond lengths of the $\{MnO_4N_2\}$ octahedron are in the range of

dx.doi.org/10.1021/cg401502f | *Cryst. Growth Des.* 2014, 14, 278−289

2.159−2.366 Å. Two such octahedra share two carboxylate groups in a bridging bidendate mode affording the formation of the $Mn_2(COO)_2$ dimer with Mn···Mn separation of 4.721 Å through adopting a nonplanar *syn−skew* coordination mode with M−O−C−C torsion angles 76.73° and 178.07°, which leads to a spiral conformation of the Mn−$(C-O-O)_2$−Mn moiety. Each $IPTA^{2-}$ acid ligand encompasses one carboxylate group in μ_2-η^1:η^1 coordination mode and the other one with μ_1-η^1:η^1 coordination mode. The connectivity of the $Mn_2(COO)_2$ dimer with $IPTA^{2-}$ acid ligand leads to the formation of an 1D metal acid chain along the crystallographic *a* axis with the separation of 10.06 Å between the two dimer units (Figure 4b). The secondary linker px3ampy implements *cis−cis−trans* conformation and is connected to the apical positions of two metal octahedra of two different $Mn_2(COO)_2$ dimeric units of adjacent chains with a separation of 8.840 Å, resulting in a $Mn_2(px3ampy)_2$ macrocycle. Along the crystallographic *b* axis, these macrocycles and the binuclear $Mn_2(COO)_2$ dimeric units are arranged alternatively by connecting at Mn(II) centers to form a chainlike structure (Figure 4c). The overall connectivity of the metal acid chains with macrocycles results in the formation of (4,4) connected 2D sheets, by considering Mn(II)-dimers as nodes and pair of macrocyles as a linker (the pair is involved in the formation of $Mn_2(px3ampy)_2$ macrocycles) and pair of $IPTA^{2-}$ ligands as an another linker. In the relevant crystal structure, each dimer is connected with four similar dimers, whereby two dimers are linked by the two $Mn_2(px3ampy)_2$ macrocycles and the other two are connected by two pairs of $IPTA^{2-}$ ligands (Figure 4d).

Important Factors That Modulate the Structural Parameters Leading to the Generation of Diverse Architectures. *Influential Role of Geometrical Disparity in H_2ADA and H_2IPTA.* The structural comparison between compounds $\{Co_2(ADA)_2(px2ampy)\}_n$ (**1**) and $\{Co_2(IPTA)_2(px2ampy)\}_n$ (**3**) reveals the consequence of replacing the ADA^{2-} from **1** by the $IPTA^{2-}$ ligand with the formation of **2** in the Co-px2ampy coordination matrix (Scheme 2). As described in the preceding section, compound **1** is characterized by a 2D coordination network, in which the Co-ADA forms paddle-wheels (SBUs) that are connected through ADA^{2-} ligand to form a 2D (4,4) connected planar sheets. On the other hand, compound **3** has a 3D network, consisting of 2D (4,4) connected Co-IPTA sheets, interlinked by px2ampy linker. Notably, in the crystal structure of compound **3**, the SBUs are Co-dimers rather than paddle-wheel SBUs, found in the crystal structure of compound **1**. The change in dimensionality from 2D (compound **1**) to 3D (compound **3**) occurs due to two different connectivity patterns of px2ampy linker with the 2D metal-acid layer in these compounds. Generally, the secondary linker px2ampy has a tendency to assist the formation of the paddle-wheels and pillar the metal acid layers to higher dimension, which has been discussed in our previous report.[14] But in the present study, in the case of compound **1**, the px2ampy linker plays a role of interweaving the metal-acid layer rather than pillaring of different layers. This unusual connectivity of the px2ampy linker in the present case can be described as an intriguing behavior of the ADA^{2-} ligand (toward px2ampy linker) compared to the other regular acid ligands due to its nonplanar twisted conformation. The coordination skeleton of the ADA^{2-} molecule allows connecting the metal polyhedra in a helical coordination pattern because of its twisted conformation. The helical coordination tendency of ADA^{2-} generates 1D zigzag chains connecting the paddle-wheel units along both axes. This conformation and connectivity of ADA^{2-} ligand create a vacant coordination strand along the 1D zigzag chain, which allows the secondary linker px2ampy to coordinate to the Co(II) centers of the paddle-wheels of the same chain in a zigzag fashion to fulfill the coordination site of the vacant strand. It is then logical to argue that the helical chain, formed by the ADA^{2-} ligand, perhaps directs the px2ampy (secondary linker) to connect along the same chain in an interweaving mode rather than pillaring the 2D ADA-paddle-wheel layer (Figure 5). It is noteworthy, here, to mention that that among the two axes of the 2D sheet, the px2ampy linker prefers to attach the vacant strand along the *b*-axis, where the SBUs are separated by a longer distance (10.334 Å) than the other axis (where the relevant separation is 8.319 Å) because it (px2ampy) is a long spacer. The conformational freedom, existing with px2ampy due to its flexibility, also stipulates its coordination in interweaving the metal centers of same plane rather than pillaring different planes (2D layers); thus the overall dimensionality is reduced to 2D rather than 3D, even though px2ampy normally acts as a pillaring component. On the other hand, in the case of compound **3**, the planar and rigid $IPTA^{2-}$ ligand connects with Co-dimers (SBUs) affording corrugated 2D sheets. In these sheets, the 1D (Co-IPTA) chains are linear in contrast to the zigzag type chains observed in the compound **1**. As a result, the px2ampy linker, in this case, is unable to

Scheme 2. Schematic Representation of Geometrical Comparison of H_2ADA and H_2IPTA Ligands

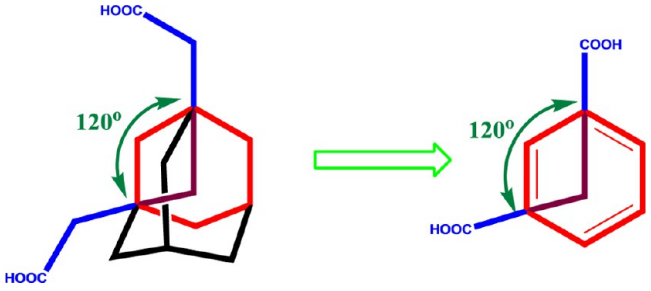

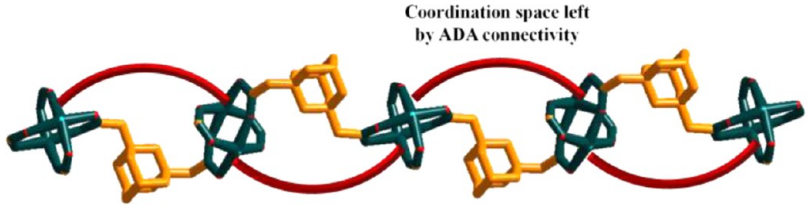

Figure 5. Figure showing the coordination space left by the ADA^{2-} connectivity for coordination with px2mpy.

dx.doi.org/10.1021/cg401502f | *Cryst. Growth Des.* 2014, 14, 278−289

interweave the metal centers of the same layer, but it highly favors pillaring the metal-acid layers (2D sheets) resulting in the formation of a 3D network. These two compounds $\{Co_2(ADA)_2(px2ampy)\}_n$ (**1**) and $\{Co_2(IPTA)_2(px2ampy)\}_n$ (**3**) can be described as unique examples to demonstrate the influence of planarity and flexibility of acid linkers to direct the coordination connectivity of a secondary linker, thereby tuning the dimensionality of final/resulting architectures.

Assessing the Influence of Metal Ionic Radii in Tuning the Dimensionality. We tried to correlate the formation of diverse architectures with different ionic radii of the metal ions used in this study. Compound $\{Cd(ADA)(px2ampy)_{0.5}\}_n$ (**2**) can be described as if it is obtained from compound $\{Co_2(ADA)_2(px2ampy)\}_n$ (**1**) by replacing the metal center Co(II) with Cd(II) in the same ADA-px2ampy coordination matrix. In the crystal structure of compound **1**, the Co(II)-ADA network forms a 2D layer with the paddle-wheel as a 4-connector node, but in the case of compound **2**, Cd(II)-ADA forms a 1D chain with Cd_2-dimer as a 2-connector node. Even though the nodes (paddle-wheel in **1** and dimer in **2**) in both compounds contain four ADA^{2-} molecules, the metal acid architectures are not identical in their respective crystal structures. A close inspection of coordination spheres of compounds **1** and **2** reveals that, around the Co(II) center (compound **1**), four carboxylate oxygen atoms from four ADA^{2-} linkers are present, whereas in the case of the Cd(II) metal center (compound **2**) five carboxylate oxygen atoms from four ADA^{2-} linkers form the coordination sphere. Compared to the ionic radius of Co^{II} ion (74 pm), the ionic radius of Cd^{II} metal ion (97 pm) is relatively larger; as a result it has tendency to adopt a higher coordination number (up to 7), or it can accommodate more bulkiness in its coordination sphere (Scheme 3). As in the case of **2**, due to

Scheme 3. Comparison of Metal Ionic Radii in the Compounds 1−4

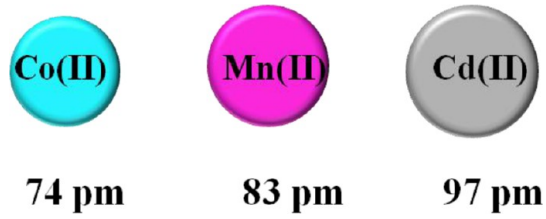

adaptability of more bulkiness in the Cd(II) coordination sphere, the ADA^{2-} molecules project most of its bulkiness around the Cd(II) center; thereby these ADA^{2-} ligands exist in nearly linear configuration with a torsion angle of 166° between both the acetate groups and forms a double chain. We wish to interpret this situation in a more logical way as in the case of compound **2**, the bulkiness of four ADA^{2-} linkers are equally distributed among three dimers (SBUs), and in the case of compound **1**, the bulkiness of four ADA^{2-} linkers are equally distributed among five paddle-wheels (SBUs) as shown in Figure 6. In this view, the crowdedness experienced by the Cd-dimer (compound **2**) is more compared to that gained by the Co-paddle-wheel (compound **1**), which in turn is reflected on the metal coordination sphere. In compound **1**, due to less adaptability of more bulkiness around a Co(II) center, the bulkiness is distributed to the other coordination spheres and thereby connectivity of ADA^{2-} forms a single chain rather a double chain in **2** (Figure 6). As explained in the previous section, the connectivity of the px2ampy linker completes coordination saturation of the second strand in a single chain to form the double chain in **1**, and in **2** it connects the already formed double chain to form a 2D layer. Generally as the ionic radius of the metal ion increases it can adopt higher coordination numbers, thereby forming a complicated or higher dimensional structures, but in the present system, as the ionic radius increases, the metal atom includes more bulkiness by concentrating the linkers in its coordination sphere and decreases the dimensionality. This observation seems to be peculiar and prompts us to study this effect in the case of compound $\{Co_2(IPTA)_2(px2ampy)\}_n$ (**3**), also. Unfortunately, we were unable to prepare the Cd analogue of compound **3**, but we could prepare the manganese analogue (where Mn^{II} (83 pm) having slightly larger ionic radius than Co^{II}) $\{Mn(IPTA)(px3ampy)\}_n$ (**4**) with pyridyl linker px3ampy which is isomeric to px2ampy (we attempted to isolate the Mn-IPTA with px2ampy but we ended up with amorphous powder). The larger ionic radius Mn^{II} always forms octahedral coordination spheres. However, Co(II) can, in general, form octahedral, square pyramidal, and tetrahedral coordination geometries. As described in the preceding section, Co-IPTA forms a 2D layer with the Co-dimer as a four-connector node (compound **3**) and Mn-IPTA forms a 1D chain with Mn_2 dimer as a two-connector node (compound **4**). It can be noted that, in the case of compound **3**, the Co-dimer consists of two different coordination spheres, i.e., octahedral $\{CoO_5N\}$ and tetrahedral $\{CoO_3N\}$. On the other hand, the Mn-dimer in compound $\{Mn(IPTA)(px3ampy)\}_n$ (**4**) consists of two identical $\{MnO_4N_2\}$ octahedral coordination spheres. This diversity makes the situation complicated to do a comparison study among these structures. In a simple way, this structural diversity can be understood as described previously: in compound $\{Co_2(IPTA)_2(px2ampy)\}_n$ (**3**), four $IPTA^{2-}$ linkers are distributed among five dimers and in compound $\{Mn(IPTA)(px3ampy)\}_n$ (**4**), four $IPTA^{2-}$ linkers are distributed to three dimers, which clearly indicates that the crowdedness around the Mn(II) center in compound **4** is higher compared to that around the Co(II) center in compound **3**. A close observation of metal centers reveals that, due to the higher coordination number exhibited by the Co(II) center (compound **3**) in terms of the number of carboxylate oxygen atoms, i.e., the existence of $\{CoO_5\}$ moiety in compound **3** compared to the existence MnO_4 moiety in **4**, a 2D metal-acid layer is found to be formed in compound **3**. But the adoptability of more bulkiness around the Mn(II) center (compound **4**) is displayed in terms of the incorporation of two bulky px3ampy linkers, which is unusual. On the whole, the structural aspects of these two compounds (**3** and **4**), in view of above observations, can be described as follows: the adoptability of more bulkiness around the Mn(II) ion (compound **4**) facilitates the incorporation of the two bulky px3ampy linkers, thereby reducing the coordination of carboxylate oxygen atoms resulting in formation of a lower dimensional structure; on the other hand, in the case of compound **3**, it incorporates only one px2ampy around the Co(II) ion in its coordination sphere and increases its carboxylate oxygen atoms resulting in the formation of a higher dimensional structure. The secondary linker px2ampy pillars the 2D metal-acid sheets in **3** to form a 3D framework, and in **4**, 1D metal-acid chains are linked by a px3ampy linker to form 2D layers, as $IPTA^{2-}$ is a rigid linker, which does not allow the pyridyl linker to connect the metal polyhedra on the same layer, as discussed in the previous section. This observation can perhaps be explained by the statement that,

dx.doi.org/10.1021/cg401502f | Cryst. Growth Des. 2014, 14, 278−289

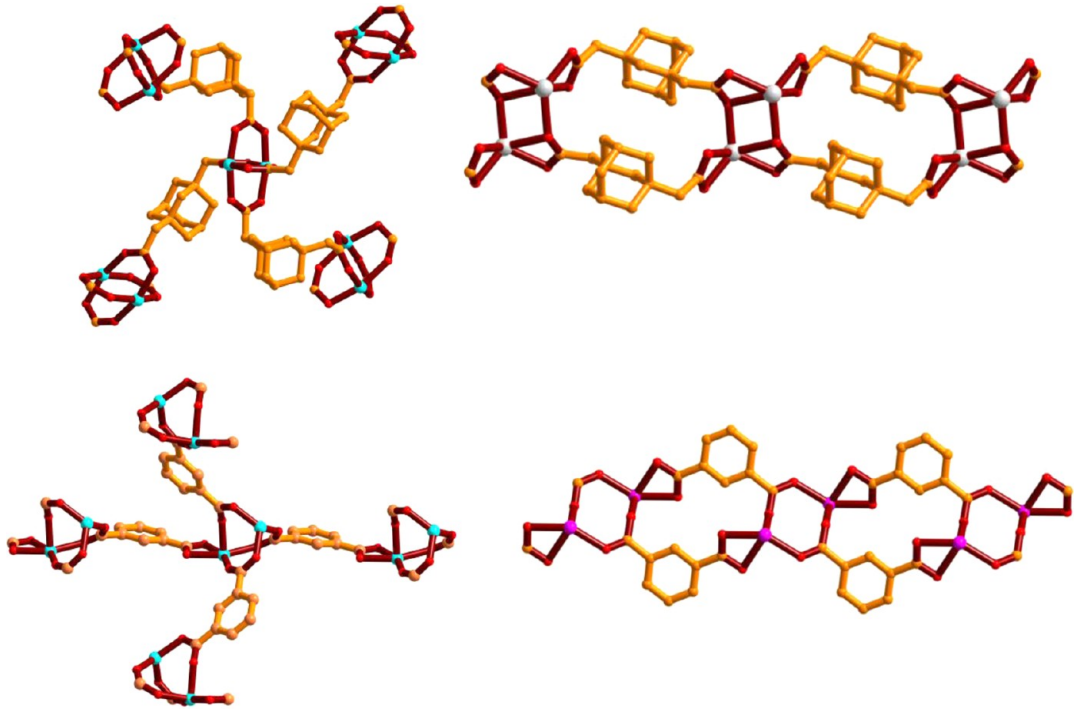

Figure 6. Distribution of bulkiness of ligands on SBUs in compounds **1**−**4**, compound **1** (top left), compound **2** (top right), compound **3** (bottom left), and compound **4** (bottom right).

Table 2. Coordination Connectivity of Compounds 1−4

C. no	M^{II}	ionic radii (pm)	metal polyhedra	SBU	linkers/SBU	M-acid dimensionality	overall dimensionality
1	Co	74	CoO_4NCo	paddle-wheel	4/5	2	2
2	Cd	97	CdO_5N	dimer	4/3	1	2
3	Co	74	CoO_5N, CoO_3N	dimer	4/5	2	3
4	Mn	83	MnO_4N_2	dimer	4/3	1	2

when different metal centers have the same coordination number, then the adoptability of bulkiness by metal center tunes the dimensionality of the resulting architecture. Whether this phenomenon is applicable to these linkers only or it can explain other similar systems is the subject of further research. The coordination connectivities in all these compounds (present study) are tabulated in Table 2.

Effect of Coordination Modes, Adopted by the Carboxylate Linkers in the Formation of SBUs. The carboxylic acid linkers, used in this study, are related to each other in terms of geometry, linker coordination angle, etc. Both the dicarboxylate ligands H_2ADA (flexible) and H_2IPTA (rigid) are ditopic; it is possible different deprotonation states, multidenticity, different coordination modes of these dicarboxylate acid ligands will have some influence on the structural diversity. In compound $\{Co_2(ADA)_2(px2ampy)\}_n$ (**1**), both the $-COO^-$ groups of the ADA^{2-} ligands adopt the μ_2-η^1: η^1 coordination mode which is the only required coordination mode for the formation of paddle-wheel secondary building units (SBUs), whereas in the case of compound $\{Cd(ADA)(px2ampy)_{0.5}\}_n$ (**2**), as we discussed in the previous section, the higher ionic radius of Cd(II) allowed more crowdedness around its coordination sphere. Hence, in this case, the carboxylate groups of ADA^{2-} ligand adopt different coordination modes in contrast to that in compound **1**. One of the carboxylate group exists in μ_1-η^1:η^1 mode and the other carboxylate group is in μ_2-η^2:η^1 mode, leading to the formation of symmetrical Cd_2-dimer instead of formation of the usual paddle-wheel. Interestingly, in the case of compound $\{Co_2(IPTA)_2(px2ampy)\}_n$ (**3**), an unusual Co-dimer is formed, (instead of Co paddle-wheel), consisting of an octahedral Co(II) coordination sphere and a tetrahedral Co(II) coordination sphere. The formation of this dimer is assisted by the two $IPTA^{2-}$ linkers which differ in coordination modes. As discussed in the structural part, both the carboxylate groups in Type I acid adopt a μ_2-η^2:η^1 mode but in Type II, one carboxylate group binds in μ_2-η^2:η^1 mode and the other one in μ_1-η^2:η^1 mode. Because of the formation of these different types of acid linkers, unsymmetrical Co_2 dimer SBU is formed rather than a symmetrical dimer. In compound $\{Mn(IPTA)(px3ampy)\}_n$ (**4**), a symmetrical Mn_2 dimer SBU has been formed with coordination modes of μ_1-η^1:η^1 and μ_2-η^1:η^1 on two carboxylate groups of the $IPTA^{2-}$. The coordination modes and respective SBUs are presented in Figure 7.

XRPD and Thermogravimetric Analysis (TGA). To ensure the phase purity of the products, X-ray powder diffraction data for the title compounds have been recorded. Similar diffraction patterns for the simulated data (calculated from single crystal data) and observed data prove the bulk homogeneity of the crystalline solids (see Supporting Information Section-1 for the PXRD patterns of compounds **1**−**4**). Although the experimental patterns have a few unindexed diffraction peaks and some are slightly broadened and shifted in comparison to those, simulated from the single-

dx.doi.org/10.1021/cg401502f | *Cryst. Growth Des.* 2014, 14, 278−289

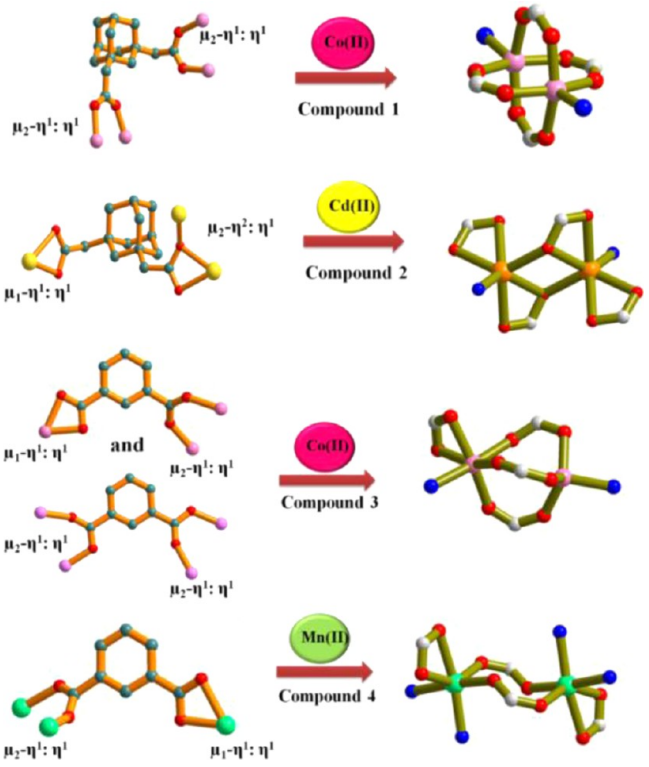

Figure 7. Coordination modes adopted by the linkers and the corresponding SBUs in compounds **1**−**4**.

crystal data, it can still be regarded that the bulk as-synthesized materials represent compounds.

TGA curves were recorded under flowing N_2 for crystalline samples **1**−**4** in the temperature range 40−1000 °C (section-2, Supporting Information). Compound **1** undergoes a significant continuous weight loss in the temperature range of the 310−610 °C attributed to the consecutive loss of the ADA^{2-} and px2ampy ligands. A gradual linear weight loss was observed in the temperature range of 610−1000 °C to the remaining weight of 19.5%, which is in accordance with the mass of CoO residue (calcd. 16.57%). The increase in weight indicates the partial decomposition at this temperature and complete decomposition at temperatures more than 1000 °C. The TGA curve of Compound **2** displays the same trend and exhibits stability up to 350 °C followed by decomposition with a weight loss up to 1000 °C. Finally, the remaining residue is presumed to be CdO (calcd. 25.34%, found 25.98%). The TGA curve of compound **3** consists of two consecutive steps of weight losses; the relevant framework is found to be stable up to 215 °C, and then it begins to collapse slowly up to 380 °C and a sharp weight loss is observed upon further heating. At 1000 °C, the remaining weight of CoO residue is 12.13% (calcd. 16.53%). For compound **4**, the continuous weight loss was observed after 320 °C, indicating the decomposition of the ADA^{2-} and px2ampy ligands. Finally, the remaining weight is 15.04% representing the MnO residue (calcd. 14.03%).

Luminescent Property of Compound 2. The fluorescent emission property of compound **2** in solid state was investigated at room temperature (section-2, Supporting Information). The free acid ligand H_2ADA does not exhibit any luminescence at the room temperature, but the bis-pyridyl ligand px2ampy exhibits emission maximum at 383 nm (upon excitation at 243 nm). Compound **2**, upon excitation at the same wavelength (243 nm, where the free px2ampy ligand was excited), exhibits a emission spectrum (of similar shape as that of free ligand) with a maximum at 392 nm (with a red shift of 9 nm in comparison to the free ligand). The emission spectrum of compound **2** may probably be assigned to the intraligand (IL) $\pi-\pi^*$ transitions, because oxidization or reduction of the d^{10} Cd(II) is difficult; thus this emission band of compound **2** cannot be attributed to metal-to-ligand charge transfer (MLCT) or ligand-to-metal charge transfer (LMCT). Interestingly, in contrast to the intensity of the emission spectrum of free ligand, the intensity of the luminescence spectrum of compound **2** has been found to be enhanced (see section 2 in Supporting Information). This phenomenon clearly indicates the fact that the flexible px2ampy ligand restrains its configuration in compound **2** and consequently reduces the degree of freedom (compared to that of free ligand), thereby reducing the loss of energy via radiationless decay.

CONCLUSION

In summary, the reactions of bent carboxylate linkers (H_2ADA and/or H_2IPTA) with long flexible pyridyl ligands along with varied transition metal ions afford four new coordination polymers with diverse topological architectures. The helical coordination tendency of H_2ADA ligand leads to formation of meso-helical M^{II}-ADA^{2-} chains in compounds **1** and **2**, and the rigid planar linker H_2IPTA results in the formation of straight M^{II}-$IPTA^{2-}$ chains in **3** and **4**. The geometrical rigidity provided by the $IPTA^{2-}$ linker facilitates the formation of a 3D framework in **3**, whereas the flexibility and planarity in the ADA^{2-} allow the formation of a 2D layer in **1**. The adoptability of bulkiness in the metal coordination sphere based on the ionic radii directs the coordination modes and connectivity patterns of the linkers, thereby influencing the final architectures, which we have attempted to discuss systematically for compounds $\{Co_2(ADA)_2(px2ampy)\}_n$ (**1**), $\{Cd(ADA)(px2ampy)_{0.5}\}_n$ (**2**), $\{Co_2(IPTA)_2(px2ampy)\}_n$ (**3**), $\{Mn(IPTA)(px3ampy)\}_n$ (**4**). In other words, the compounds, presented in this study, are designed systematically to highlight the geometrical restraints of the angular linkers in terms of planarity and flexibility and finally to explore the hidden role of metal ionic radii in the self-assembly of coordination networks.

ASSOCIATED CONTENT

Supporting Information

Crystallographic data in CIF format, PXRD patterns, TGA plots, photoluminescent spectra of compound **2**, selected bond distances and angles in PDF format. This information is available free of charge via the Internet at http://pubs.acs.org.

AUTHOR INFORMATION

Corresponding Author

*E-mail: skdsc@uohyd.ernet.in, samar439@gmail.com; fax: +91-40-2301-2460; tel: +91-40-2301-1007.

Notes

The authors declare no competing financial interest.

ACKNOWLEDGMENTS

The authors thank the CSIR, Government of India (Project No. 01(2556)/12/EMR-II) for financial support. The National X-ray Diffractometer facility at University of Hyderabad by the Department of Science and Technology, Government of India, is gratefully acknowledged. We are grateful to UGC, New

Delhi, for providing infrastructure facility at University of Hyderabad under UPE Grant. P.M. and B.K.T. thank CSIR, India respectively for their fellowships.

REFERENCES

(1) (a) Ma, S. Q. *Pure Appl. Chem.* **2009**, *81*, 2235. (b) Ma, X.; Champness, N.; Schröder, M. Hydrogen, Methane and Carbon Dioxide Adsorption in Metal-Organic Framework Materials. In *Functional Metal-Organic Frameworks: Gas Storage, Separation and Catalysis*; Schröder, M., Ed.; Topics in Current Chemistry series; Springer: Berlin, 2010; Vol. *293*, p 35.

(2) (a) Roques, N.; Mugnaini, V.; Veciana, J. *Top. Curr. Chem.* **2010**, *293*, 207. (b) Huang, Y. G.; Jiang, F. L.; Hong, M. C. *Coord. Chem. Rev.* **2009**, *253*, 2814. (c) Kurmoo, M. *Chem. Soc. Rev.* **2009**, *38*, 1353. (d) Zeng, Y. F.; Hu, X.; Liu, F. C.; Bu, X. H. *Chem. Soc. Rev.* **2009**, *38*, 469.

(3) (a) Allendorf, M. D.; Bauer, C. A.; Bhakta, R. K.; Houk, R. J. T. *Chem. Soc. Rev.* **2009**, *38*, 1330. (b) Schuth, F.; Sing, K. S. W.; Weitkamp, J. *Handbook of PorousSolids*; Wiley-VCH: New York, 2002. (c) Valtchev, V.; Mintova, S.; Tsapatsis, M. *Ordered Porous Solids: Recent Advances and Prospects*; Elsevier B.V.: Oxford, 2009.

(4) (a) Cho, S. H.; Ma, B.; Nguyen, S. T.; Hupp, J. T.; Albrecht-Schmitt, T. E. *Chem. Commun.* **2006**, 2563. (b) Alkordi, M. H.; Liu, Y.; Larsen, R. W.; Eubank, J. F.; Eddaoudi, M. *J. Am. Chem. Soc.* **2008**, *130*, 12639. (c) Nuzhdin, A. L.; Dybtsev, D. N.; Bryliakov, K. P.; Talsi, E. P.; Fedin, V. P. *J. Am. Chem. Soc.* **2007**, *129*, 12958. (d) Wu, C. D.; Hu, A.; Zhang, L.; Lin, W. *J. Am. Chem. Soc.* **2005**, *127*, 8940.

(5) Stupp, S. I.; Braun, P. V. *Science* **1997**, *277*, 1242.

(6) (a) Shin, D. M.; Lee, I. S.; Chung, Y. K. *Inorg. Chem.* **2003**, *42*, 8838. (b) Han, S. S.; Deng, W. Q.; Goddard, W. A. *Angew. Chem., Int. Ed.* **2007**, *46*, 628.

(7) Li, H.; Eddaoudi, M.; Groy, T. L.; Yaghi, O. M. *J. Am. Chem. Soc.* **1998**, *120*, 8571.

(8) Zhang, B.; Clearfield, A. *J. Am. Chem. Soc.* **1997**, *119*, 2751.

(9) Mietrach, A.; Muesmann, T. W. T; Christoffers, J.; Wickleder, M. S. *Eur. J. Inor. Chem.* **2009**, *35*, 5328.

(10) Lin, P.; Clegg, W.; Harrington, R. W.; Henderson, R. A. *Dalton Trans.* **2005**, *14*, 2388.

(11) (a) Dai, F.; Dou, J.; He, H.; Zhao, X.; Sun, D. *Inorg. Chem.* **2010**, *49*, 4117. (b) Li, G.; Lu, J.; Li, X.; Yang, H.; Xu, B.; Cao, R. *CrystEngComm* **2010**, *12*, 3780.

(12) Henke, S.; Schneemann, A.; Wütscher, A.; Fischer, R. A. *J. Am. Chem. Soc.* **2012**, *134*, 9464.

(13) (a) Schaate, A.; Klingelhofer, S.; Behrens, V.; Wiebcke, M. *Cryst. Growth Des.* **2008**, *8*, 3200. (b) Liu, Y.; Qi, Y.; Lv, Y. Y.; Che, Y. X.; Zheng, J. M. *Cryst. Growth Des.* **2009**, *9*, 4797. (c) Li, Z. X.; Hu, T. L.; Ma, H.; Zeng, Y. F.; Li, C. J.; Tong, M. L.; Bu, X. H. *Cryst. Growth Des.* **2010**, *10*, 1138. (d) Yang, J.; Ma, J. F.; Battern, S. R.; Su, Z. M. *Chem. Commun.* **2008**, 2223. (e) Pachfule, P.; Dey, C.; Panda, T.; Banarjee, R. *CrystEngComm* **2010**, *12*, 1600.

(14) (a) Tripuramallu, B. K.; Manna, P.; Reddy, S. N.; Das, S. K. *Cryst. Growth Des.* **2012**, *12*, 777. (b) Manna, P.; Tripuramallu, B. K.; Das, S. K. *Cryst. Growth Des.* **2012**, *12*, 4607. (c) Tripuramallu, B. K.; Mukherjee, S.; Das, S. K. *Cryst. Growth Des.* **2013**, *13*, 2426.

(15) (a) Yang, W.; Lin, X.; Blake, A. J.; Wilson, C.; Hubberstey, P.; Champness, N. R.; Schröder, M. *Inorg. Chem.* **2009**, *48*, 11067. (b) Li, S. L.; Lan, Y. Q.; Ma, J. F.; Yang, J.; Wei, G. H.; Zhang, L. P.; Su, Z. M. *Cryst. Growth Des.* **2008**, *8*, 675. (c) Han, L.; Zhou, Y.; Zhao, W. N.; Li, X.; Liang, Y. X. *Cryst. Growth Des.* **2009**, *9*, 660.

(16) (a) Huang, B. F.; Xiao, H. P.; Huang, H.; Li, X. H.; Wang, J. G.; Morsali, A. *J. Coord. Chem.* **2013**, *66*, 904. (b) Wang, X. F.; Zhang, Y. B.; Xue, W. *Cryst. Growth Des.* **2012**, *12*, 1626. (c) Zhang, W. H.; Wang, Y. Y.; Lermontova, E. Kh.; Yang, G. P.; Liu, B.; Jin, J. C.; Dong, Z.; Shi, Q. Z. *Cryst. Growth Des.* **2010**, *10*, 76.

(17) (a) Hamblin, J.; Tuna, F.; Bunce, S.; Childs, L. J.; Jackson, A.; Errington, W.; Alcock, N. W.; Nierengarten, H.; Dorsselaer, A. V.; Leize-Wagner, E.; Hannon, M. J. *Chem.—Eur. J.* **2007**, *13*, 9286. (b) Mondal, R.; Bhunia, M. K.; Dhara, K. *CrystEngComm* **2008**, *10*, 1167. (c) Son, S. U.; Park, K. H.; Kim, B. Y.; Chung, Y. K. *Cryst. Growth Des.* **2003**, *3*, 507.

(18) (a) Jin, J. C.; Wang, Y. Y.; Liu, P.; Liu, R. T.; Ren, C.; Shi, Q. Z. *Cryst. Growth Des.* **2010**, *10*, 2019. (b) Jin, J. C.; Wang, Y. Y.; Zhang, W. H.; Lermontov, A. S.; Lermontova, E. Kh.; Shi, Q. Z. *Dalton Trans.* **2009**, 10181. (c) Zhang, W. H.; Wang, Y. Y.; Lermonntova, E. Kh.; Yang, G. P.; Liu, B.; Jin, J. C.; Dong, Z.; Shi, Q. Z. *Cryst. Growth Des.* **2010**, *10*, 76. (d) Zhang, W. H.; Wang, Y. Y.; Ren, C.; Wen, G. L.; Guo, C. Y.; Shi, Q. Z. *Inorg. Chem. Commun.* **2009**, *12*, 1011. (e) Zhang, W. H.; Dong, Z.; Wang, Y. Y.; Hou, L.; Jin, J. C.; Huang, W. H.; Shi, Q. Z. *Dalton Trans.* **2011**, *40*, 2509.

(19) (a) Wang, X.; Luan, J.; Lin, H.; Lu, Q.; Xu, C.; Liu, G. *Dalton Trans.* **2013**, *42*, 8375. (b) Jiménez, A. R.; García, R. L.; Lozada, A. C.; Hernández, S.; Apan, T. R.; NietoCamacho, A.; Gómez, E. *J. Organomet. Chem.* **2013**, *738*, 10. (c) Yáñez, S. P.; Beobide, G.; Castillo, O.; Cepeda, J.; Luque, A.; Roman, P. *Cryst. Growth Des.* **2013**, *13*, 3057−3067.

(20) (a) Deng, Z. P.; Qi, H. L.; Huo, L. H.; Ng, S. W.; Zhaoa, H.; Gao, S. *Dalton Trans.* **2010**, *39*, 10038. (b) Deng, Z. P.; Zhu, L. N.; Gao, S.; Huo, L. H.; Ng, S. W. *Cryst. Growth Des.* **2008**, *8*, 3277. (c) Deng, Z. P.; Huo, L. H.; Qi, H. L.; Zhu, L. N.; Zhao, H.; Gao, S. *CrystEngComm* **2011**, *13*, 4218. (d) Deng, Z. P.; Huo, L. H.; Qi, H. L.; Zhao, H.; Gao, S. *Inorg. Chem. Commun.* **2011**, *14*, 64.

(21) (a) Zhu, L. N.; Gao, S.; Huo, L. H. *Acta Crystallogr., Sect. E: Struct. Rep. Online* **2007**, *E63*, o4459. (b) Zou, R. Y.; Xu, F. B.; Li, Q. S.; Song, H. B.; Lv, H.; Zhang, Z. Z. *Acta Crystallogr., Sect. E: Struct. Rep. Online* **2003**, *E59*, o1312.

(22) (a) *SAINT: Software for the CCD Detector System*; Bruker Analytical X-ray Systems, Inc.: Madison, WI, 1998. (b) Sheldrick, G. M. *SADABS: Program for Absorption Correction*; University of Gottingen: Gottingen, Germany, 1997. (c) Sheldrick, G. M. *SHELXS-97: Program for Structure Solution*; University of Gottingen: Gottingen, Germany, 1997. (d) Sheldrick, G. M.*SHELXL-97: Program for Crystal Structure Analysis*; University of Gottingen: Gottingen, Germany, 1997. (e) Blatov, V. A.; Shevchenko, A. P.; Serezhkin, V. N. *J. Appl. Crystallogr.*, **2000**, *33*, 1193. TOPOS software is available for download at http://www.topos.ssu.samara.ru.